References and Notes

1. E. L. Powers, R. B. Webb, C. F. Ehret, *Radiat. Res.* **2**, 94 (1960).
2. E. L. Powers, in *Electron Spin Resonance in the Effect of Radiation on Biological Systems* (Nuclear Science Report No. 43, National Academy of Sciences–National Research Council, Washington, D.C., 1966), p. 137.
3. A. Tallentire and E. L. Powers, *Radiat. Res.* **20**, 270 (1963).
4. A. Tallentire, A. B. Jones, G. P. Jacobs, *Isr. J. Chem.* **10**, 1185 (1972).
5. M. H. Cross, M. Simic, E. L. Powers, *Int. J. Radiat. Biol.* **24**, 207 (1973).
6. D. Ewing, *ibid.* **28**, 165 (1975).
7. E. L. Powers, Fifth Symposium on Microdosimetry, Verbania-Pallanza, Italy, 22 to 26 September 1975, in press.
8. D. Ewing, *Radiat. Res.* **59**, 156 (1974).
9. L. M. Dorfman and G. E. Adams, *NSRDS-NBS Report No. 46* (National Bureau of Standards, Department of Commerce, Washington, D.C., 1973).
10. E. L. Powers and M. Cross, *Int. J. Radiat. Biol.* **17**, 501 (1970).
11. We thank H. Haydon and J. Maynard for their technical help. This work was supported by ERDA E-AT-(40-1)-3408 and PHS GM-13557.

* Present address: Department of Radiation Therapy and Nuclear Medicine, Hahnemann Medical College and Hospital, Philadelphia, Pa. 19102.

16 March 1976; revised 13 August 1976

Comet West and the Scattering Function of Cometary Dust

Abstract. *Observations of Comet West (1975n) at wavelengths from 0.5 to 18 microns and at a variety of scattering angles are used to infer the scattering phase function for the cometary dust. This function is strongly peaked in the forward direction. The form of the function indicates that the particles are dielectric grains with radii of approximately 1 micron. Abrupt increases in the intrinsic brightness of the coma (both in scattered sunlight and in thermal emission) are consistent with the projected times of comet fragmentation.*

Observations of the comae, tails, and antitails of comets made at wavelengths λ from 0.5 to 20 μ have given new information about the constitution of the grains and limits on the sizes of grains present in comets Bennett (1970II) (*1*), Kohoutek (1973f) (*2*), Bradfield (1974b) (*3*), and Kobayashi-Berger-Milon (1975h) (*4*). The discovery of the silicate feature at λ = 10 and 20 μ in the first three of these comets demonstrated that silicate grains less than 5 μ in diameter were present. In addition, the antitail of Comet Kohoutek and the coma of Comet Kobayashi-Berger-Milon did not show the silicate signature, an indication that larger particles with diameters in excess of 20 μ were present, as predicted for the antitail of Comet Kohoutek by Sekanina (*5*).

Comet West afforded a unique opportunity to study another aspect of cometary dust which could be diagnostic. This is the light scattering or albedo of the dust as a function of the scattering angle. For the other comets mentioned the scattering angle θ observed was near 90°, but, because Comet West passed between the earth and the sun, forward scattering angles as small as 34° were observed.

Our measurements were made with a square diaphragm projecting a beam (20 by 20 arc seconds) centered on the coma, and the uniform background radiation from the sky was canceled by beam switching through an angle of 30 arc seconds. The same bolometer system was used at all wavelengths from 0.5 to 18 μ to guarantee that the comet colors were

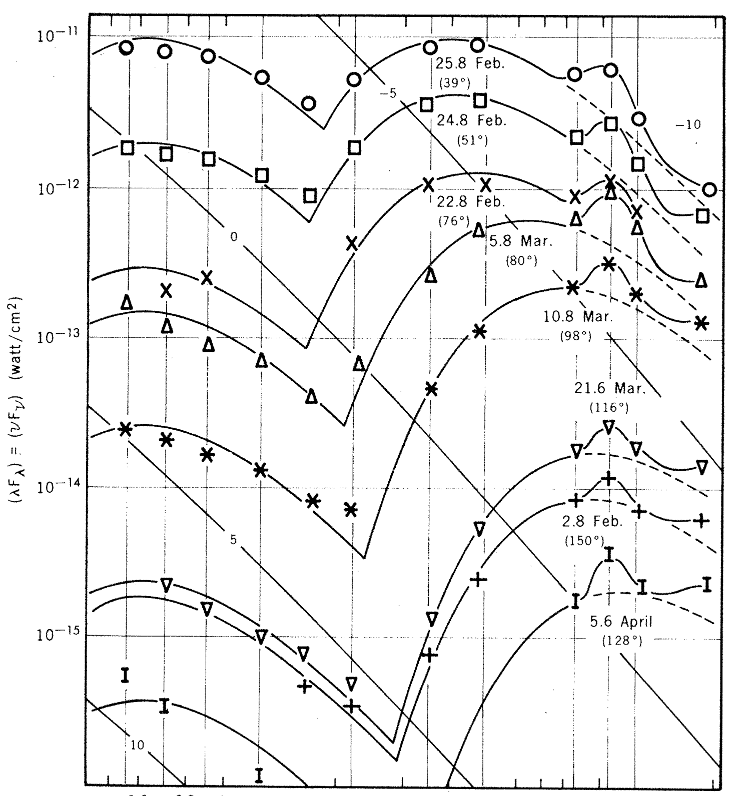

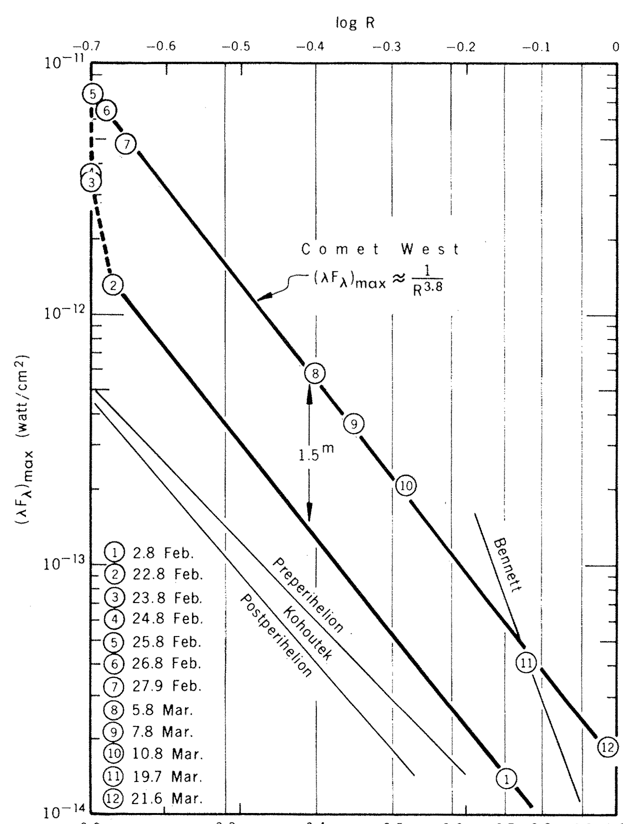

Fig. 1 (left). The energy distribution of Comet West (ν is frequency) between 2.8 February and 5.6 April. The silicate feature at 10 μ is always in evidence. The short-wavelength fluxes are due to scattered sunlight and the long-wavelength fluxes to thermal radiation. The forward scattering is shown by the increased brightness of the scattered light relative to the thermal emission at small scattering angles, for example, on 25.8 February. The scattering angles are given in parentheses below the dates. Fig. 2 (right). A plot of the thermal emission of the comet as a function of heliocentric distance. The effect of fragmentation is shown by the abrupt increase in brightness between observations 2 and 3 and observations 4 and 5.

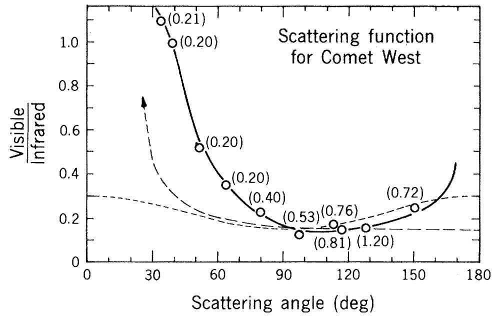

Fig. 3. The observed ratio of the reflected to the emitted flux of the comet as a function of scattering angle. This ratio is proportional to the scattering phase function of the dust. Qualitatively correct comparison curves expected for Rayleigh scattering with $X = 2\pi a/\lambda \ll 1$ (small dashes) and larger ($X = 7$) conducting (iron) grains (large dashes) and dielectric grains (solid line) are shown as discussed in the text. Heliocentric distances (in astronomical units) are shown in parentheses.

measured with the same coma geometry. The comet fragmented into four pieces near perihelion (*6*), and the intrinsic brightness of the coma increased (presumably because of the increase in the total nuclear surface area). The simultaneous increase in both the observed flux of scattered sunlight at short wavelengths and the thermal radiation at longer wavelengths comes from the dust, and the four fragments producing this dust were always within our beam.

Figure 1 shows the energy distribution for Comet West between 2.8 February and 5.6 April 1976. The relative magnitudes of the energy in reflected sunlight and thermal radiation are indicated by the blackbody curves fitted through the points. The silicate signature is superimposed on the thermal blackbody curve. The blackbody temperature of the grains increases smoothly as the comet approaches the sun, reaching a temperature of 920°K on 25.8 February.

The value of $(\lambda F_\lambda)_{max}$ for the thermal reradiation is plotted in Fig. 2 as a function of R, the distance from the sun to the comet. Two increases in intrinsic brightness occurred near perihelion, one between 22.8 and 23.8 February and the other between 24.8 and 25.8 February. These brightness increases are due to the fragmentation, and the fragmentation times are in fair agreement with those inferred by Sekanina (*6*).

The visual flux from the coma of Comet West was dominated by a continuum due to scattered sunlight rather than by discrete emission lines (*7*). The reflected light appeared to have approximately solar colors; the colors of the infrared emission were seen to vary smoothly before and after perihelion with the 10-μ silicate emission band always present, an indication that no radical change in the nature of the grains had occurred. Hence, since both the scattered and the emitted energies measured sample the same volume of dust, their ratio $T(\theta)$ is simply proportional to the scattering phase function for the grains and is properly normalized for the direct comparison of conditions at various scattering angles during the cometary orbit. This scattering phase function can be compared with that expected for dielectric and conducting grains of various characteristic sizes. Figure 3 shows that the observed scattering function is asymmetric with a marked tendency toward forward scattering. Clearly non-Rayleigh scattering dominates, and the scattering properties of larger particles of radius a for which

$$X = \frac{2\pi a}{\lambda} \gtrsim 1$$

must be investigated. The optical properties of such larger particles are determined by the complex index of refraction

$$m = n - ik$$

which can be wavelength-dependent. Comparison with published phase diagrams based on Mie theory calculations such as those of van de Hulst (*8*), Deirmendjian *et al.* (*9*), Hansen and Pollack (*10*), Hanner (*11*), and Wickramasinghe (*12*), as well as the laboratory measurements of Holland and Draper (*13*) and Holland and Gagne (*14*), suggest that the observed scattering phase function is best fitted by dielectric materials (where $1.3 \leqslant n \leqslant 2.0$ and $n \gg k$) such as dirty ice or silicates with $6 \leqslant X \leqslant 15$. Good conductors such as iron ($n \approx k$) are characterized by relatively flat phase functions outside the immediate vicinity of forward scattering. The phase diagrams for dielectrics of fixed radii are characterized by sharp resonances which are smoothed out when a distribution of radii is present. The situation is illustrated in Fig. 3 where Rayleigh scattering and the generalized result for larger particles, a dielectric and a conductor [taken from Deirmendjian *et al.* (*9*)], are shown. The theoretical curves are smoothed and the comparisons are meant to be qualitative rather than quantitative. Graphite, according to the definitions used here, is neither a dielectric nor a good conductor, and its presence is not completely ruled out by the data available. No unique fit seems possible over the region of the phase diagram samples.

One can determine the bolometric Bond albedo A by integrating the observed ratio T over all solid angles

$$\frac{A}{1 - A} = \frac{1}{2}\int_0^\pi T(\theta)\sin\theta d\theta$$

In earlier analyses, following O'Dell (*15*), the phase dependence of scattering has been neglected. At phase angles near 90°, $T \approx 0.18$ for Comet West as well as for the other comets mentioned. Hence, if isotropic scattering is assumed, $A \sim 0.15$. Integration over the incomplete phase diagram between 30° and 150° yields a lower limit to A of $\gtrsim 0.22$. The assumption that T is constant outside the region observed ($T = 1.1$ for $\theta < 30°$ and 0.2 for $\theta > 150°$) raises the total albedo to $A \gtrsim 0.27$, which is nearly twice that inferred when isotropy was assumed. Examination of representative phase diagrams for dielectric materials suggests that a significant fraction (but less than or on the order of a half) of the total grain scattering occurs outside the range $30° \leqslant \theta \leqslant 150°$ sampled in the present observations. Hence $A \sim 0.3$ to 0.5 is a conservative estimate. Comet grains appear to be fairly good absorbers ($k \gtrsim 0.05$) by comparison with the poorly absorbing relatively "clean" core-mantle grains of ices and perfect crystal silicates commonly modeled [for example, see Aannestad (*16*)].

Knowledge of the scattering properties of cometary grains is important, not only in identifying grain composition but also in applying the results of observations of real grains to radiative transfer calculations of circumstellar dust shells. Scattering from cometary grains is anisotropic with strongly enhanced forward scattering. As Jones has recently illustrated (*17*), such forward scattering reduces the effective albedo of cloud material, allowing considerable optical flux to escape an otherwise optically thick cloud. Spectra computed for model circumstellar dust shells in steady-state radiative equilibrium around cool stars require that the silicate grains be at least moderately good absorbers of visible and near-infrared radiation (*18*). Such "dirty" grains might be similar to the dielectric silicate material present in Comet West.

Combined visible and infrared observations of Comet West have provided a unique opportunity to separate and examine two factors governing the surface brightness of comets. (i) Fragmentation, which increases the amount of material exposed to sunlight, results in an increase in both reflected and emitted radiation while the ratio of the reflected to the emitted radiation remains relatively constant. (ii) The marked asymmetry in the scattering phase function noted for comet grains allows large increases in the ratio of reflected to emitted radiation during the orbital interval of forward scattering. The onset of forward scattering geometry along a cometary orbit can lead to dramatic increases in the visual brightness of the comet. The coma of Comet West was easily seen through finder telescopes at perihelion roughly 7° from the sun. The grains observed include dielectrics with the characteristic 10-μ signature commonly attributed to silicates and are fairly good absorbers of visible radiation. These comet grains are apparently physically quite similar to the material detected in the varied environments of circumstellar and interstellar space.

EDWARD P. NEY
K. M. MERRILL
School of Physics and Astronomy, University of Minnesota, Minneapolis 55455

References and Notes

1. R. Maas, E. P. Ney, N. J. Woolf, *Astrophys. J. Lett.* **160**, L101 (1970).
2. E. P. Ney, *ibid.* **189**, L141 (1974); G. H. Rieke and T. A. Lee, *Nature (London)* **248**, 737 (1974); I. Gatley, E. E. Becklin, G. Neugebauer, M. W. Werner, *Icarus* **23**, 561 (1974).
3. E. P. Ney, *Icarus* **23**, 551 (1974).
4. ——, *Bull. Am. Astron. Soc.* **7** (No. 4), 508 (1975).
5. Z. Sekanina, *Icarus* **23**, 502 (1974).
6. ——, *Sky Telescope* **1976**, 386 (June 1976).
7. G. H. Herbig, personal communication.
8. H. C. van de Hulst, *Light Scattering by Small Particles* (Wiley, New York, 1957).
9. D. Deirmendjian, R. Clasun, W. Vierzee, *J. Opt. Soc. Am.* **51**, 620 (1961).
10. J. E. Hansen and J. B. Pollack, *J. Atmos. Sci.* **27**, 265 (1970).
11. M. S. Hanner, *Astrophys. J.* **164**, 425 (1971).
12. N. C. Wickramasinghe, *Light Scattering Functions with Applications in Astronomy* (Wiley, New York, 1973).
13. A. C. Holland and J. S. Draper, *Appl. Opt.* **6**, 511 (1967).
14. A. C. Holland and G. Gagne, *ibid.* **9**, 1113 (1970).
15. C. R. O'Dell, *Astrophys J.* **166**, 675 (1971).
16. A. Aannestad, *ibid.* **200**, 30 (1975).
17. T. W. Jones, *Publ. Astron. Soc. Pac.* **85**, 811 (1973).
18. —— and K. M. Merrill, *Astrophys. J.*, in press.
19. This work was supported by NASA and NSF grants. We thank J. Stoddart and B. Hatfield for assistance with the observations.

14 July 1976

Mammal Teeth from the Forest Marble (Middle Jurassic) of Oxfordshire, England

Abstract. *A very early stage in the evolution of the talonid basin is seen in a eupantothere lower molar from the Upper Bathonian of central England. The corresponding upper molars and the first known Middle Jurassic morganucodontid, kuehneotheriid, and dryolestid teeth are briefly described and illustrated.*

The mammals arose from reptilian ancestors near the end of the Triassic period and persisted as several distinct groups of small unspecialized animals throughout the remainder of the Mesozoic era. The modern orders of therian mammals then arose from one of these archetypal groups (the Eupantotheria) by rapid radiative evolution in Late Cretaceous and Early Cenozoic times. Only this therian radiation is well documented in the fossil record, the critical early steps of mammalian evolution in the Mesozoic being very poorly known. For example, after their first occurrence in the Rhaeto-Lias (~ 190 million years ago), mammalian fossils do not again occur in any abundance until the Upper Jurassic, a stratigraphic gap that represents 40 million years. Only two localities of intermediate age have previously yielded fossil mammals, both dated to the Bathonian (~ 165 million years ago, Middle Jurassic) (*1*, *2*).

I have recently discovered another three mammal-bearing sites of Middle Jurassic age (*3*, *4*), of which the most productive has been a bed of nonmarine clay within the Forest Marble formation (Upper Bathonian) of Kirtlington, Oxfordshire, England (*5*). Wet-sieving of this sediment has produced numerous teeth (34 from 0.27 m^3) that provide significant new information on the early stages of mammalian evolution. In particular, the order Eupantotheria is represented by fossils of at least three families, one of which, the Peramuridae, known previously only from the Late Jurassic, appears to lie close to the main line of therian evolution.

Order Eupantotheria Kermack and Musset

Family (?) Peramuridae Kretzoi

Genus *Palaeoxonodon* (nov.)

Diagnosis: Lower molar with small but distinct "posterior accessory cusp" (*6*) on the crista obliqua, which forms a continuation of the distal metaconid crest and runs distobuccally into a prominent talonid cusp. Anterobuccal cingulum only weakly developed, if at all. Referred upper molars with prominent metacone and stylocone, and distinct "cusp c."

Species *ooliticus* (nov.)

Diagnosis: As for genus. Upper Bathonian.

Holetype: Author's collection (*7*), No. FM/K8 (Fig. 1, a and b). Lower right molar has two subequal roots. Paraconid is broken. Protoconid is high and has a mesial edge which recurves sharply at its midpoint; its lingual face is planar, giving the protoconid a roughly semicircular cross section. The large, erect talonid cusp has a concave lingual face, which forms a part of a shallow talonid basin situated on the lingual side of the crista obliqua. The distolingual rim of this basin bears two barely perceptible swellings, which judging by their positions, may be incipient developments of a hypoconulid and an entoconid.

Referred specimens: Incomplete lower molar FM/K7; here only one talonid cusp is present, which is quite unbasined.

Three upper molars (FM/K4, FM/K12, FM/K30) are referred to *P. ooliticus* chiefly because they are similar in size to the two lower molars. The best preserved of these (Fig. 1c) has a high paracone on whose distal flank is a smaller, but well-defined metacone, the two cusps sharing a common base. A metacrista runs distobuccally from the apex of the metacone, bearing three small cusps, the largest of which is directly distobuccal to the metacone. In this position, it seems to correspond with the virtually obsolete "cusp c" in Crompton's (*8*) figure of the *Peramus* upper molar. The stylocone is only slightly smaller than the metacone, and is significantly larger than the stylocone of *Peramus*.

Another type of eupantothere upper molar (Fig. 2, a and b) is somewhat larger than and shows distinct differences in structure from those referred to *P. ooliticus*. For example, the parastylar region is relatively larger, producing a pronounced hooklike structure at the anterobuccal corner of the tooth. The metacrista bears only two cusps, but these are more clearly defined than in the referred *P. ooliticus* upper molars. Finally, the metacone does not share a common base with the paracone and is more distobuccally situated, in which feature it somewhat resembles Mills' (*6*) reconstruction of the upper molar of *Amphitherium*.

The dryolestids, hitherto known from the Late Jurassic and Early Cretaceous, are represented by two rootless lower molars, both of which show the anteroposterior compression of the crown typical of the family. Their talonids are broken off, but must have been small structures situated low on the distal flank of the metaconid. Both specimens have a well-developed anterobuccal cuspule (see Fig. 2, d to f).

An incomplete symmetrodont lower molar (Fig. 2c) strongly resembles those of both *Kuehneotherium* (Rhaeto-Lias) (*9*) and the Middle Jurassic amphilestids (*1*). This suggests that the latter are symmetrodonts (order Eupantotheria) as was proposed by Mills (*10*), and not triconodonts, as is usually thought.

The true triconodonts are represented in the new fauna primarily by a well-preserved lower molar of a morganucodontid (Fig. 2g), which is larger and has a